Scientific Reports

https://doi.org/10.1038/s41598-026-47971-z

Article in Press

Gambogic acid-loaded transferrin-modified liposomes enhancing potent ferroptosis in breast cancer

Received: 3 December 2025

Accepted: 6 April 2026

Published online: 10 April 2026

Cite this article as: Rong W., Zhang M., Yang S. *et al.* Gambogic acid-loaded transferrin-modified liposomes enhancing potent ferroptosis in breast cancer. *Sci Rep* (2026). https://doi.org/10.1038/s41598-026-47971-z

Wenqing Rong, Minquan Zhang, Siqi Yang, Kaiwen Wang, Xiaoping Yang, Guolei Zhang, Zhe Li, Yue Ding, Tong Zhang, Yun Gai & Jinshuai Lan

Gambogic acid-loaded transferrin-modified liposomes enhancing potent ferroptosis in breast cancer

Wenqing Rong[#1], Minquan Zhang[#2], Siqi Yang[#3], Kaiwen Wang[1], Xiaoping Yang[1], Guolei Zhang[1], Zhe Li[2,3], Yue Ding[2,3], Tong Zhang[*2,3], Yun Gai[*1], Jinshuai Lan[*1,2]

[1] Shanghai Seventh People's Hospital, Shanghai 200137, China

[2] School of Pharmacy, Shanghai University of Traditional Chinese Medicine, Shanghai 201203, China

[3] State Key Laboratory of Integration and Innovation of Classic Formula and Modern Chinese Medicine, Shanghai University of Traditional Chinese Medicine, Shanghai 201203, China

[#]These authors have contributed equally to Ffigthis work

*Correspondence:

E-mail address: zhangtongshutcm@hotmail.com (Tong Zhang), gaiyunlucky@163.com (Yun Gai), lanjinshu-ai_shut@126.com (Jinshuai Lan)

Abstract

Breast cancer (BC), the most common cancer in women, is closely related to ferroptosis, which is an iron-dependent form of cell death. Gambogic acid (GA), the main active ingredient extracted from the dry resin secreted by Garcinia cambogia, can effectively induce ferroptosis in tumor cells. However, its application is limited by poor water solubility, short half-life, and vascular irritation. Moreover, the sensitivity of cells to ferroptosis is positively correlated with the concentration of intracellular iron ions, which based on transferrin (Tf)-Tf receptor (TfR) pathway. Increasing intracellular iron ions within tumor cells may enhance GA-induced ferroptosis. Based on the high expression of TfR in tumor cells, Tf can be both a tumor-target modification and an Fe^{3+} carrier. Therefore, GA-loaded Tf-modified liposomes (GA@Tf-Lip) with pH-responsive properties were developed. GA@Tf-Lip increased the intracellular iron ion content of MCF-7 cells, promoted the Fenton reaction to increase the level of ROS, downregulated the GSH content, and accelerated lipid peroxide accumulation. The distribution of the formulation by *in vivo* imaging experiments showed that the prepared GA@Tf-Lip had a higher drug accumulation at tumor sites and exhibited a good antitumor effect by promoting ferroptosis. Overall, GA@Tf-Lip exerted a good anti-BC effect, which is expected to provide a new strategy for the treatment of BC and the clinical transformation of GA.

Keywords

Gambogic acid; Transferrin; Ferroptosis; Target drug delivery; Breast cancer

1 Introduction

Breast cancer (BC) is the second most prevalent and fatal malignancy in women, and has become a major global health challenge[1]. According to the latest Global Cancer Observatory (GLOBOCAN) estimates, there are 670000 deaths globally due to BC by 2022[2]. It is predicted that this number may increase to over 3 million new cases and 1 million deaths every year by 2040[3]. Current clinical treatment methods, including surgery, chemotherapy, and radiation, and new therapeutic techniques, such as molecular-targeted therapy and immunotherapy, have also been applied in BC treatment[4]. However, these treatment methods are limited by high tumor recurrence rates and multidrug resistance.

As an iron-dependent form of cell death, ferroptosis has emerged as a promising therapeutic target in oncology, particularly BC[5]. Ferroptosis can not only regulate the growth and proliferation of tumor cells but also has obvious advantages in overcoming the drug resistance of traditional cancer treatment drugs[6]. Current ferroptosis inducers, including sorafenib[7], erastin[8], and RSL3[9], have already been used as clinical drugs, but their therapeutic effects are still limited by serious adverse reactions caused by low tumor-targeting effects. With the development of nanotechnology, nanodrug delivery systems have opened new horizons for BC treatment. Some nano systems have already been developed for BC treatment[10–12], and others have been designed specifically for inducing ferroptosis by releasing $Fe^{2+/3+}$ at the tumor site[13–15]. However, the application of these nano systems is limited by their complex preparation process, low tumor-targeting effect, and severe side effects. Moreover, the use of exogenous iron ions may cause problems in iron ion metabolism *in vivo*.

Gambogic acid (GA) is extracted from the traditional Chinese medicine Garcinia Hanburyi Hook. and has been studied for multiple cancer treatments[16]. However, the application of GA is limited by its low water solubility, quick clearance *in vivo* and adverse side effects such as vascular stimulation and bellyache[17]. Transferrin (Tf) is a non-heme iron-bound β-globulin related to Fe uptake and cell growth. Cancer cells have an increased iron requirement to meet their demand for growth compared to normal cells, and the expression of Tf-receptor (TfR) are high to make TfR an effective target[18]. In this study, we developed Tf-modified liposomes (GA@Tf-Lip) loaded with GA to induce ferroptosis in BC cells. GA@Tf-Lip was prepared from 1,2-Dioleoyl-sn-glycero-3-phosphoethanlamine (DOPE), which undergoes a lamellar-to-hexagonal phase transition under acidic conditions, promoting liposomal destabilization and accelerated drug release at tumor sites[19]. The Tf-modification enables GA@Tf-Lip to release GA at targeted sites through the TfR-mediated pathway and increase the intracellular Fe content, enhancing GA-induced ferroptosis in BC cells.

Current ferroptosis-related carriers including natural protein nanocages, metal-coordinated nano assemblies and biomimetic nanocarriers. But these carriers have many limitations, such as natural nanocages are unstable in the blood circulation, metal-coordinated nano assemblies are dependent on the specific molecular structure of the drug which must have a group that can coordinate with metals, and the production of biomimetic nanocarriers is cumbersome and the yield is low. What's more, they also have potential safety problems because they all increase Fe ion in tumor cells by introducing exogenous iron ions. The developed GA@Tf-Lip use Tf to bind endogenous iron ions to target tumor cells and enhancing ferroptosis, and liposomes are currently more mature preparations and are easier for clinical translation.

There are also some GA delivery systems including metal polyphenol coordination nanoparticles (GA-Fe), functionalized liposomes (folic acid) and prodrug delivery system[20,21]. Compared to these drug delivery systems, the GA@Tf-Lip have some obvious advantages. First, targeting TfR is generally more efficient and specific so that the GA@Tf-Lip have a higher tumor-target effect. Second, the construction of liposomes is relatively simpler and more standardized, the threshold for industrial production is lower, and the possibility of clinical transformation is higher. Third, the developed GA@Tf-Lip use Tf to bind endogenous iron ions, which avoid potential iron metabolism disorders and other safety issues.

In conclusion, the developed GA@Tf-Lip is an effective drug delivery system with several advantages. First, GA@Tf-Lip had a nanoparticle size, so it could accumulate in tumor sites via the enhanced permeability and retention (EPR) effect, and the GA@Tf-Lip can rapidly degrades under acidic conditions while the Tf modified on liposomes could further precisely target tumor cells by Tf-TfR binding. Second, GA can directly induce ferroptosis in BC cells[22], the therapeutic effect of ferroptosis is commonly limited by endogenous iron ion insufficiency, whereas the developed GA@Tf-Lip could bind free Fe^{3+} i*n vivo* to increase the Fe^{2+} concentration in tumor cells. Third, the elimination of GA@Tf-Lip *in vivo* was slower, and GA@Tf-Lip decreased the side effects of GA. In brief, we developed a novel Tf-modified GA-loaded nanosystem for BC treatment that could provide a reference for clinical GA applications.

2 Materials and Methods

2.1 Reagents

GA and cholesterol hemisuccinate were purchased from Shanghai Aladdin Biochemical Technology Co., Ltd, DOPE and Distearoyl phosphoethanolamine-PEG2000 (DSPE-MPEG2000) were purchased from Avito (Shanghai) Pharmaceutical Technology Co., Ltd.; DSPE-mPEG2000-Tf was purchased from Guangzhou Weihua Biotechnology Co., Ltd; Dulbecco's Modified Eagle Medium (DMEM), Fetal Bovine Serum (FBS), Penicillin-Streptomycin, Trypsin-EDAT(0.25%), and trypsin were purchased from Thermo Fisher Scientific CN, Endothelial Cell Medium (ECM) was purchased from ScienCell Research Laboratories. 1.25% tribromoethanol was purchased from Nanjing Aibei Biotechnology Co.,Ltd. Sodium pentobarbital was purchased from Merck Investment (China)Co.,Ltd.

2.2 Cells and Animals

Cells: Michigan Cancer Foundation-7 (MCF-7) cells were purchased from Cell Bank of Chinese Academy of Sciences. MCF-7 cells were seeded in T25 cell culture flasks in DMEM medium containing 10% fetal bovine serum (FBS) and 1% penicillin-streptomycin (PS) in a sterile cell culture incubator containing 5% CO_2 at 37°C.

Animals: Thirty-four BABL/C-Nude female mice（age: 4 weeks, weight: 16-18 g）and twelve New Zealand rabbits （half male/half female, age: 8-9 weeks, weight: 1.9-2.2 kg） were purchased from Shanghai SLAC Laboratory Animal Co.,Ltd. All animals were maintained in a temperature-controlled and humidity-controlled facility (25 ± 2℃, 50 ± 5% relative humidity) under a 12 h light/dark cycle with unrestricted access food and water. All the evaluations were made by blinded observers. If the animal dies or the tumor volume exceeds 2000 mm^3, the data is excluded. All the animals were randomly divided into different groups, and random numbers were generated using the standard = RAND() function in Microsoft Excel. At the end of the experiments, the mice were euthanized by intraperitoneal injection of excessive 1.25% tribromoethanol (20 μL/g), the rabbits were euthanized via intraperitoneal injection of excessive sodium pentobarbital (100 mg/kg). All experimental procedures were approved by the Animal Ethics Committee of Shanghai University of Traditional Chinese Medicine (PZSHUTCM2309080007, PZSHUTCM2309110010)

2.3 Preparation of GA@Tf-Lip

DOPE, DSPE-PEG2000, Chems and GA were mixed according to the massage ratio ratio (6:0.5:4:0.4) and dissolved completely in an appropriate amount of methanol: chloroform mixed solution (v: v = 1:1). The solution was evaporated under reduced pressure in a water bath at 60 °C to obtain a uniform phospholipid film. The eggplant flask was placed overnight in a vacuum desiccator to remove the organic solvent completely. An appropriate amount of phosphate buffered saline (PBS) with DSPE-PEG2000-Tf (DSPE-PEG2000-Tf: DOPE = 1:3000) was added to obtain a final GA concentration of 333 μg/mL. After 20 min of hydration at 60 °C, the solution was ultrasonicated (80 W, 3 s on/2 s off, 10 min) in an ice water bath to form GA@Tf-Lip. GA@Lip was prepared using the same method but without DSPE-PEG2000-Tf.

2.4 Characterization of GA@Tf-Lip

Particle size was determined using a Zetasizer Nano ZS ZEN3600 (Malvern Instruments, Worcestershire, UK). For the particle morphology, a JEM-2100 transmission electron microscope (TEM) (Japan Electronics Co., Ltd., Osaka, Japan) provided a larger view. Drug content (%) and encapsulation rate (%) were measured at 360 nm by high performance liquid chromatography (HPLC) (Agilent 1200 series HPLC, Agilent Technologies Inc.). The samples were collected after free GA was separated in ultrafiltration tube by centrifugal separation. The drug content and encapsulation rate was calculated based on equations: Drug content(%)=(GA mass in liposomes/liposomes mass) × 100%, Encapsulation rate(%)= (GA mass in liposomes/feeding GA mass) × 100%. The chromatographic column was a Dikma C18 column (250 mm × 4.6 mm, 5 μm) with a mobile phase of methanol: 0.1% acetic acid water (93:7) at a flow rate of 1 mL/min and a column temperature of 25 °C. The stability of the prepared liposomes were also evaluated, GA@Lip and GA@Tf-Lip were stored at 4 °C until further use. The particle size, PDI, and encapsulation rate of GA@Lip and GA@Tf-Lip were measured after 1, 3, and 7 d, respectively.

2.5 *In vitro* drug release

In vitro drug release experiment was performed, and the concentration of GA in the different media was determined using HPLC. GA solution (1 mL of GA solution, GA@Lip, and GA@Tf-Lip were added to 9 mL of different media (pH 5.5, 6.8, and 7.4). The samples were placed in a thermostatic shaker (37 °C, 100 rpm), and 0.5 mL of samples were taken at 0.5, 1, 2, 4, 6, 8, 12 and 24 h, respectively. After sampling, the corresponding dissolution medium (0.5 mL) was added. The samples were centrifuged at 13000 rpm for 10 min and the supernatant was collected for HPLC analysis to calculate the drug release percentage.

2.6 Cell cytotoxicity study

MCF-7 cells in the logarithmic growth phase were seeded at a density of 8× × 10^4 cells/mL in 96-wells plates (100 μL per well) and cultured overnight. GA, GA@Lip, GA@Tf-Lip, and GA@Tf-Lip + Fe^{3+} were diluted into multiple concentration gradients (0, 0.25, 0.5, 0.75, 1, 1.25, 1.5, and 2 μM GA) in DMEM without FBS or PS. Different media (100 μL) were then added to each well. After incubation at 37 °C for 24 h, 10 μL of cell counting kit-8 (CCK-8) was added. After incubation for 1 h, the absorbance was measured at 450 nm using a microplate reader (Thermo Fisher Microplate Reader, Thermo Fisher Scientific CN) to calculate the cell viability and IC_{50} of each group. The cell viability was calculated using the following formula:

$$\text{Cell viability} = (OD_t - OD_0) / (OD_c - OD_0) \times 100\%$$

Where OD_t is the sample absorbance, OD_c is the reference absorbance, and OD_0 is the absorbance of the DMEM.

2.7 Cell apoptosis study

MCF-7 cells in the logarithmic growth phase were seeded at a density of 5 × 10^5 cells/mL in six-well plates and cultured overnight (2 mL per well). GA, GA@Lip, GA@Tf-Lip, and GA@Tf-Lip + Fe^{3+} were diluted to 1 μM (in terms of GA) in DMEM without FBS and PS, and 2 mL of the different media was added to each well. After incubation at 37 °C for 24 h, the cells were trypsinized and resuspended in 100 μL of Binding Buffer. The samples were incubated at 4 °C for 30 min after mixing with 5 μL of

AnnexinV-FITC and 5 μL of propidium iodide. After incubation, the samples were detected in the FITC and PE channels by flow cytometry.

2.8 Live-Dead cell staining

MCF-7 cells in the logarithmic growth phase were seeded at a density of 5 × × 10^5 cells/mL in confocal dishes and cultured overnight (1 mL per confocal dish). GA, GA@Lip, GA@Tf-Lip, and GA@Tf-Lip + Fe^{3+} were diluted to 1 μM (in terms of GA) in DMEM without FBS or PS. One milliliter of different media was added to the corresponding confocal dish, and the control group was treated with DMEM without FBS or PS. After incubation for 24 h, 1 mL of Calcein-AM/PI detection solution was added, incubated for 30 min at 37 °C. The samples were washed three times with PBS, and the images were observed using CLSM. The parameters were set as follows: calcein-AM λ_{ex} = 494 nm, λ_{em} = 517 nm. PI: λ_{ex} = 535 nm, λ_{em} = 617 nm.

2.9 Cellular uptake study

MCF-7 cells in the logarithmic growth phase were seeded at a density of 5 × 10^5 cells/mL in six-well plates and cultured overnight (2 mL per well). 1,1'-dioctadecyl-3,3',3'-tetramethylindocarbocyanine perchlorate (DiI) was used as the marker. DiI, DiI@Lip, and DiI@Tf-Lip were diluted to 1 μM (in terms of DiI) using a DEME without FBS or PS. Two milliliters of different media were added to each well. After incubation at 37 °C for 24 h, the cells were trypsinized with EDTA-free trypsin and resuspended in PBS. The samples were detected in the PE channels using flow cytometry (BD Facscalibur Flow Cytometry, Becton, Dickinson, and Company).

MCF-7 cells in the logarithmic growth phase were seeded at a density of 5 × 10^5 cells/mL in confocal dishes and cultured overnight (1 mL per dish). DiI, DiI@Lip, and DI@Tf-Lip were diluted to 1 μM (in terms of DiI) using DEME without FBS and PS, and 1 mL of each medium was added to the corresponding confocal dish. After incubation at 37 °C for 8 h, the confocal dishes were washed with PBS three times and 0.5 mL of Hoechst 33342 staining solution was added. After incubation at 37 °C for 30 min, the staining solution was discarded and the confocal dishes were washed three times with PBS. Images were obtained using a confocal laser scanning microscope (CLSM). The parameters were set as follows: DiI, λ_{ex}=549 nm, λ_{em}=565 nm; Hoechst 33342, λ_{ex}=346 nm, and λ_{em}=460 nm.

2.10 The ability of GA@Tf-Lip to induce ferroptosis in MCF-7 cells

2.10.1 Intracellular Fe^{2+} concentration study

MCF-7 cells in the logarithmic growth phase were seeded at a density of 5 × 10^5 cells/mL in six-well plates and cultured overnight (2 mL per well). Fe^{3+}, GA+Fe^{3+}, GA@Lip + Fe^{3+} and GA@Tf-Lip + Fe^{3+} were diluted to 1μM (in terms of GA) in DMEM without FBS or PS. Two milliliters of different media was added to the corresponding wells, and the control group was only treated with DMEM without FBS and PS. After incubation for 24 h, 1 mL of FerroOrange solution (1 μM) was added, incubating at 37 °C for 30 min. Cells were collected by ethylenediaminetetraacetic acid-free trypsinization and detected in the PE channel by flow cytometry.

2.10.2 Detection of indicators of oxidative stress

The levels of malondialdehyde (MDA), glutathione (GSH), and glutathione peroxidase 4 (GPX4) were measured to evaluate their ability to promote ferroptosis in MCF-7 cells. MDA is a product of

ferroptosis and is metabolized by lipid peroxidation[23]. GSH plays an important role in inducing ferroptosis, and its consume of GSH promotes lipid peroxidation and accelerate ROS production of ROS[24,25]. GPX4 is an antioxidant defence enzyme that can repair oxidative damage and is a major inhibitor of ferroptosis[26].

MDA and GSH levels were determined using ELISA. MCF-7 cells in the logarithmic growth phase were seeded at a density of 5×10^5 cells/mL in six-well plates and cultured overnight (2 mL per well). GA, GA@Lip and GA@Tf-Lip + Fe^{3+} were diluted to 1 μM (in terms of GA) by DMEM without FBS and PS. Two milliliters of different media was added to the corresponding wells, and the control group was only treated with DMEM without FBS and PS. After incubation at 37 °C for 24 h, the medium in each well was discarded, the cells were scraped using a cell scraper, and the levels of MDA, GSH, and GPX4 in cells in each group were determined the corresponding ELISA kits.

GPX4 levels were determined using western blot (WB). The cells were collected using a cell scraper and lysed to quantify protein concentrations. 1/4 volume of the 5 × loading buffers was added to the remaining samples. The samples were mixed, heated at 100 °C for 5 min, and stored at -80 °C for further WB analysis, and the luminescence imaging system was used for imaging and photography.

2.10.3 Mitochondrial membrane potential study

MCF-7 cells in the logarithmic growth phase were seeded at a density of $5 \times \times 10^5$ cells/mL in confocal dishes and cultured overnight (1 mL per confocal dish). GA, GA@Lip, GA@Tf-Lip, and GA@Tf-Lip+Fe^{3+} were diluted to 1μM (in terms of GA concentration) in DMEM without FBS or PS. One milliliter of different media was added to the corresponding confocal dish, and the control group was treated with DMEM without FBS or PS. After incubation for 24 h, 1 mL of JC-1 staining solution was added, incubated for 30 min at 37 °C. The samples were washed three times with PBS, and the images were observed using CLSM. The parameters were set as follows: J-monomer λ_{ex}=514 nm and λ_{em}=529 nm. J-aggregates: λ_{ex}=585 nm and λ_{em}=590 nm.

2.11 *In vitro* hemolysis study

Two milliliters of blood were collected from male SD rats and centrifuged at 3000 rpm for 30 min at 4 °C. The supernatant was discarded and 2 times of saline were added for saline until the supernatant was removed. The separated red blood cells were resuspended in an appropriate amount of saline and stored at 4 °C.

The red blood cell suspensions were divided into five groups: H_2O, PBS, GA, GA@Lip, and GA@Tf-Lip. One milliliter of the corresponding medium was added to 20 μL of the red blood suspension. After incubation at 37 °C for 30 min, the solution was centrifuged at 3000 rpm and the color of the supernatant was recorded. The ultraviolet absorption of each group was determined at 540 nm and the hemolysis rate of each group was calculated according to the following formula:

Relative hemolysis rate = $(OD_{treat} - OD_{nc}) / (OD_{pc} - OD_{nc}) \times 100\%$.

Where OD_{treat} is the absorbance of the preparation group, OD_{pc} is the absorbance of the H_2O group, and OD_{nc} is the absorbance of the PBS group.

2.12 Vascular irritation experiments

According to the principle of equivalent dose conversion, a dose of GA (1.5 mg/kg) was selected for vascular irritation experiments. Twelve New Zealand rabbits (half male and half female) were randomly divided into four groups (n = 3): control group (saline), GA Group (1.5 mg/kg), GA@Lip group (GA 1.5 mg/kg), and GA@Tf-Lip group (GA 1.5 mg/kg). The drugs were injected through the left marginal ear vein after the rabbits were anesthetized via intraperitoneal injection of 30 mg/kg of sodium pentobarbital. The rabbits were administered drugs every two days for a total of 10 days.

24 h after the last administration, the rabbits were euthanized via intraperitoneal injection of excessive sodium pentobarbital (100 mg/kg) until death, and the left ear of each rabbit was fixed with 4% paraformaldehyde for 24 h for H&E staining analysis. Histological examination was performed under a light microscope and photographs were taken. The criteria used were redness, swelling, hyperemia, induration, necrosis, degeneration, and inflammatory cell infiltration.

2.13 Establishment of an *in vivo* MCF-7 orthotopic tumor model

0.1 mL of MCF-7 cells suspension (5×10^7 cells/mL) were injected under the second pair of papillae on the right side of nude mice. Tumor patches were observed subcutaneously at the injection site 3-5 days after inoculation, proving that the mouse MCF-7 orthotopic tumor model was successfully constructed.

2.14 *In vivo* biodistribution and anti-tumor activity of liposomes

When the tumor size reached 200 mm^3, mice were randomly divided into three groups (n = 3): ICG, ICG@Lip, and ICG@Tf-Lip. 200 μL of ICG, ICG@Lip, and ICG@Tf-Lip were intravenous injected in mice (ICG 2.5 mg/kg). The mice were photographed 1, 2, 4, 6, 8, and 24 h after administration using a live imaging system after anesthetizing the mice with 1.5% isoflurane. After 24 h of imaging, the mice were immediately euthanized by intraperitoneal injection of excessive 1.25% tribromoethanol (20 μL/g), and their hearts, livers, spleens, lungs, kidneys, and tumors were imaged. The parameters were set as follows: ICG, λ_{ex} = 620 nm, λ_{em} = 650 nm.

2.15 *In vivo* anti-tumor effect of GA@Tf-Lip

When the tumor volume was approximately 50 mm^3, the mice were randomly divided into five groups (five mice in each group): control group, doxorubicin (DOX) group (DOX 2 mg/kg), GA group (GA 3 mg/kg), GA@Lip group (GA 3 mg/kg), and GA@Tf-Lip group (GA 3 mg/kg). The mice were administered drugs via intravenous injection, and the tumor volume and body weight were measured every two days for a total of 14 days. The day after the last administration, the mice in each group were euthanized by intraperitoneal injection of excessive 1.25 % tribromoethanol (20 μL/g), and the heart, liver, spleen, lung, and kidney were collected and stored at -80 °C for further analysis, including immunofluorescence analysis and the measurement of the contents of Fe^{2+}, ROS, lipid peroxides (LPO), GPX4, and Ki67 in tumors. A portion of the heart, liver, spleen, lung, kidney, and tumor from each group of mice was removed, fixed with 4% paraformaldehyde for 48 h for hematoxylin and eosin (H&E) staining, and photographed under a microscope.

2.16 Statistical analysis

All data are presented as mean ± SD, unless otherwise stated. One-way ANOVA and Student's t-tests was used to assess statistical significance using Prism 9 for MacOS (version 9.3.1). The following terms were used to indicate statistical significance: $^{*}P < 0.05$, $^{**}P < 0.01$, $^{***}P < 0.001$, $^{*}\# < 0.05$, $^{**}\# < 0.01$, $^{***}\# < 0.001$.

3 Results and Discussion

3.1 Characterization of GA@Lip and GA@Tf-Lip

As shown in **Fig. 1A&1B**, the prepared GA@Lip was a clear yellow solution with a narrow particle size distribution (108.8 ± 1.6 nm, n = 3), a low PDI (0.140 ± 0.013, n = 3) and a stable zeta potential (-28.3 ± 2.0 mV, n = 3), while the particle size distribution of GA@Tf-Lip was 119.9 ± 1.0 nm (n = 3), PDI was 0.188 ± 0.017 (n = 3) and zeta potential was -32.7 ± 3.7 mV (n = 3). According to the HPLC analysis, the drug loading and encapsulation rate of GA@Lip are 2.94 ± 0.12% and 99.7 ± 0.1%, the drug loading and encapsulation rate of GA@Tf-Lip were 2.89 ± 0.20% and 99.8 ± 0.1%. We also measured the stability data of GA@Lip and GA@Tf-Lip under light-protected conditions at 4 °C in 7 days, and the results are shown in **Table S1**. The results show that the developed GA@Lip and GA@Tf-Lip all have a good stability. The TEM results are shown in **Fig. 1C**. The prepared GA@Lip and GA@Tf-Lip were spherical in shape. The prepared GA@Lip and GA@Tf-Lip were clearly defined and spherical in shape. Compared to GA@Lip, GA@Tf-Lip had a larger particle size owing to the outer coating of a layer of DSPE-PEG2000-Tf, which was consistent with the results measured by the Malvern particle sizer. At pH 5.5, the phospholipid bilayer on the surface of the two liposomes ruptured, and the boundary was unclear, indicating that the prepared GA@Lip and GA@Tf-Lip were pH-sensitive and broke under acidic conditions.

Liposomes containing Chems exhibit pH-responsive drug release behavior[27], solutions with pH = 5.5, 6.8, and 7.4, were selected for *in vitro* release experiments to evaluate whether GA@Tf-Lip exhibited pH-responsive drug release behavior. The release results are shown in **Fig. 1D-1F**, under different pH conditions, all free GA was released within 1 h. The cumulative release of GA@Lip and GA@Tf-Lip at pH 7.4 was only 32.96% ± 0.9% and 31.83% ± 3.1% after 1 h, respectively, indicating that the release of GA could be significantly slowed down by loading GA into liposomes. The cumulative release rates of GA@Lip at pH = 5.5, 6.8 and 7.4 for 1 h were 60.26%, 58.59%, 33.7%, while the cumulative release rates of GA@Tf-Lip at pH = 5.5, 6.8 and 7.4 were 62.92%, 52.8% and 35.51%. Different kinetic modeling were established and the data were fitted, and the results are shown in **Table S2-S4**. The fitting results show that the mechanism of drug release of GA@Lip and GA@Tf-Lip is First-order release at pH 7.4 and pH 6.8, while it is more fit to erosion at pH 5.5, which indicates that the developed liposomes have a pH-sensitive drug release effect. The results indicated that there was a significant difference in the release rate of the two pH-responsive liposomes under neutral and acidic conditions, and that the acidic environment could significantly accelerate the disintegration of liposomes and release of drugs.

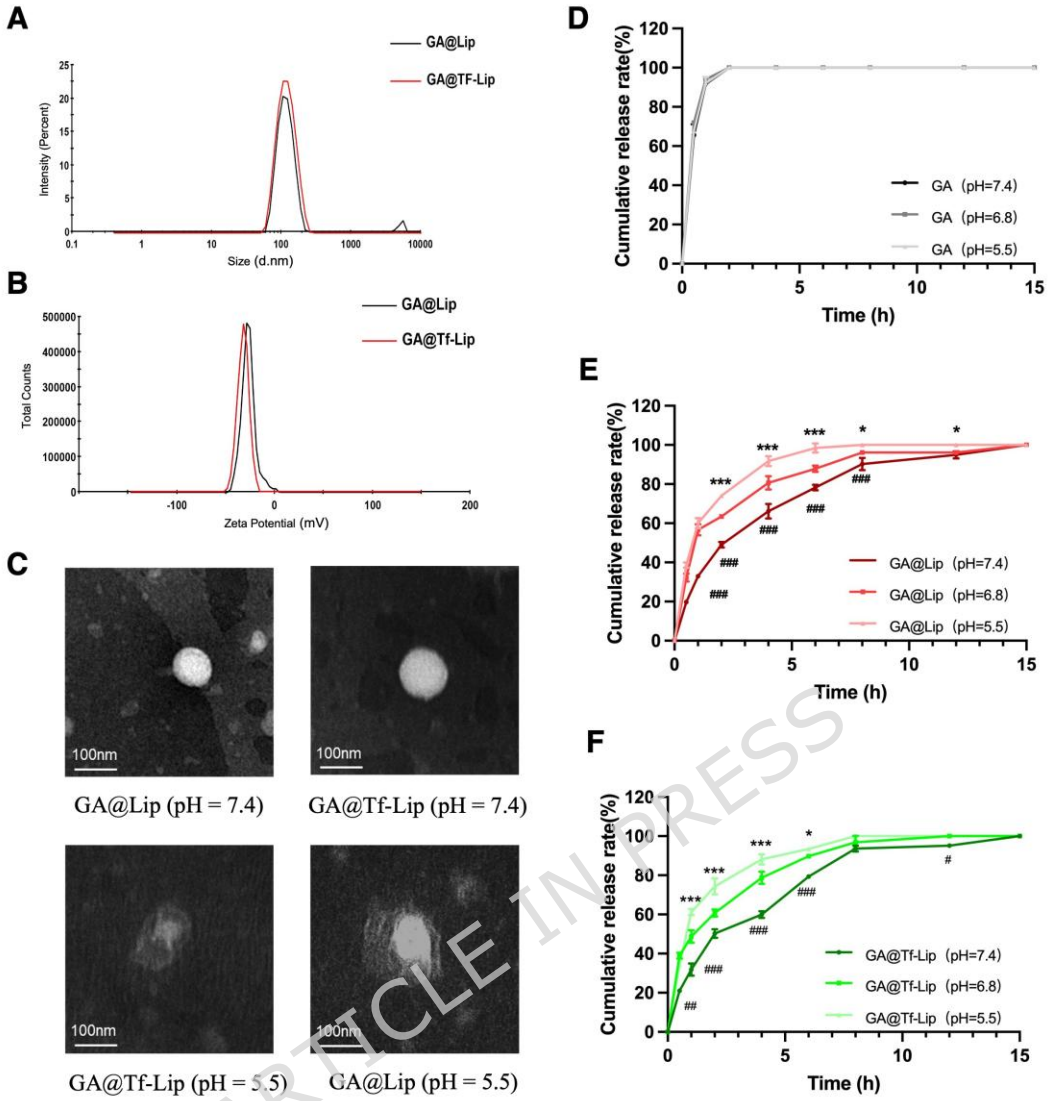

Fig. 1 Characterization of GA@Lip and GA@Tf-Lip. (A) Particle size of GA@Lip and GA@Tf-Lip, (B) Zeta potential of GA@Lip and GA@Tf-Lip, (C) TEM analysis, (D) *In vitro* release of GA under different pH condition (n = 3), (E) *In vitro* release of GA@Lip under different pH condition (n = 3), (F) *In vitro* release of GA@Tf-Lip under different pH condition (n = 3). (Significant differences between pH = 5.5 and pH = 6.8: $^{*}P < 0.05$, $^{**}P < 0.01$, $^{***}P < 0.001$. Significant differences between pH = 7.7 and pH = 6.8: $^{\#}P < 0.05$, $^{\#\#}P < 0.01$, $^{\#\#\#}P < 0.001$.)

3.2 *In vitro* anti-tumor effect of GA@Tf-Lip

CCK-8 assay was used to detect the cytotoxicity of MCF-7 cells in each group, and the results are shown in **Fig. 2A**. The IC_{50} values of GA, GA@Lip, GA@Tf-Lip, and GA@Tf-Lip+Fe^{3+} in the MCF-7 cells were 1.34 μM, 1.14 μM, 0.88 μM, and 0.66 μM. The rate of cell proliferation inhibition in MCF-7 cells was positively correlated with drug concentration. The cytotoxicity of GA@Lip was approximately 1.2 times higher than that of GA, GA@Tf-Lip was approximately 1.5 times higher than that of GA, and GA@Tf-Lip + Fe^{3+} was approximately 1.3 times higher than that of GA@Tf-Lip, which indicated Fe^{3+} can enhance the anti-tumor ability of GA@Tf-Lip by inducing ferroptosis. These results suggest that transferrin-modified liposomes could enhance the cytotoxicity of GA, and that the toxicity of the preparation to tumor cells was stronger in the Fe^{3+}-containing tumor microenvironment.

The apoptosis results are shown in **Fig. 2B&2C**, the MCF-7 cells induced apoptosis after administration, and the trend was consistent with the cytotoxicity experiment. The total apoptosis rates were 0.18 ± 0.02% (Control group), 39.66 ± 0.26% (GA group), 43.05 ± 1.57% (GA@Lip group), 65.91 ± 1.17% (GA@Tf-Lip group), 78.12 ± 2.16% (GA@Tf-Lip + Fe^{3+} group). The results showed that GA@Tf-Lip has a better ability of inducing apoptosis than GA and GA@Lip, and Fe^{3+} enhanced GA@Tf-Lip-induced apoptosis.

Calcein AM produces green fluorescence and can easily penetrate the membrane of living cells[28], and is often used to stain living cells. Propidium iodide (PI) is a nucleic acid fluorescent dye that fluoresces red[29] and is often used to indicate cells or dead cells with damaged cell membranes. The results of live-dead cell staining are shown **Fig. 2D&2E**, with almost no red fluorescence (PI staining) in the control group and different intensities of red fluorescence in each administration group. The fluorescence intensity of GA@Tf-Lip and GA@Tf-Lip + Fe^{3+} was significantly higher than that of the other groups, indicating that the prepared GA@Tf-Lip had an enhanced antitumor effect compared to GA and GA@Lip, which was consistent with the results of the cytotoxicity and apoptosis experiments.

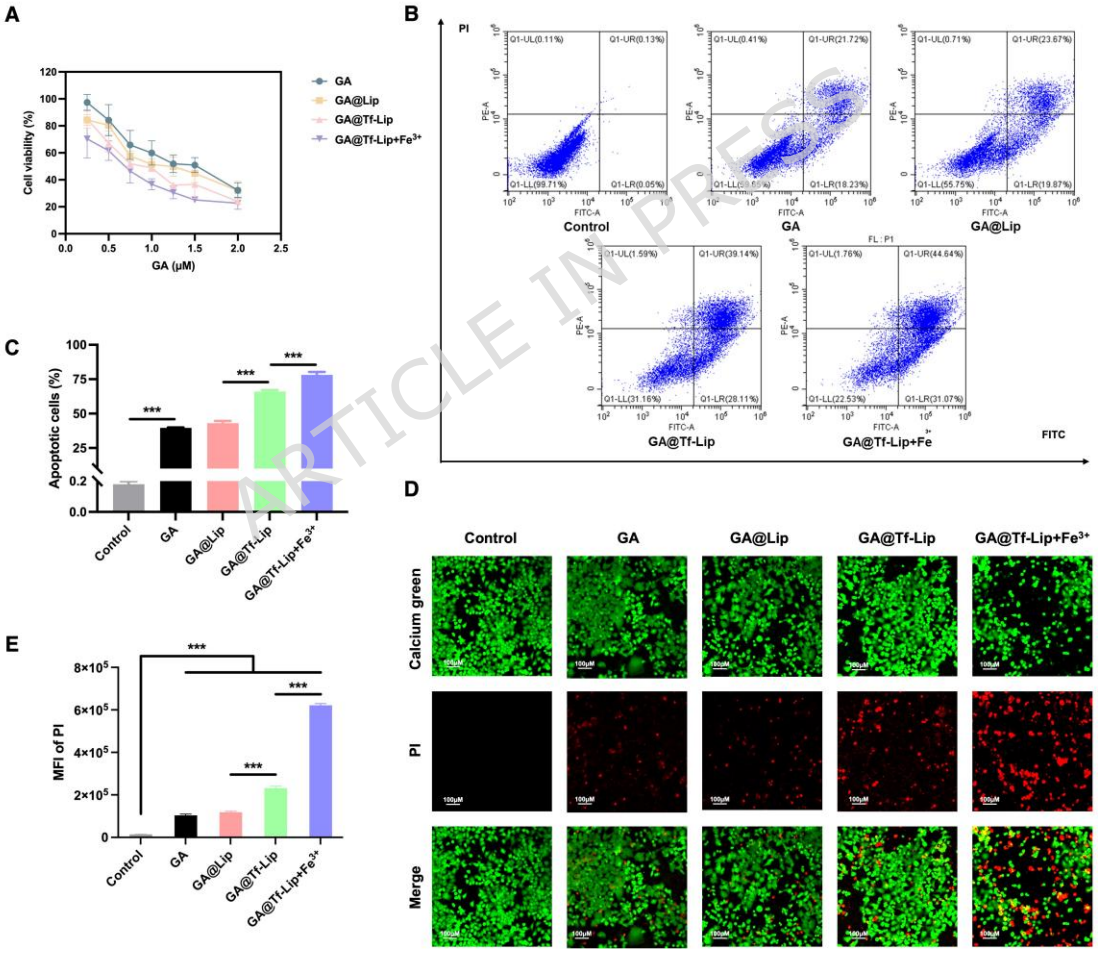

Fig. 2 *In vitro* anti-tumor effect of GA@Tf-Lip. (A) Cell viability of MCF-7 cells after 24 h (n = 3), (B) Cell flow cytometry results of apoptosis in MCF-7 cells(n = 3), (C) Live/dead viability assays (Calcein AM^+ + PI^+) in different groups (n = 3), (D) CLSM results of live-dead cell staining (100 μm), (E) Semi-quantitative analysis of PI staining in CLSM pictures (n = 3). (Significant difference: $^*P < 0.05$, $^{**}P < 0.01$, $^{***}P < 0.001$.)

3.3 Cellular uptake study

DiI is a lipophilic membrane dye often used to label lipid membrane structures. Liposomes have a phospholipid bilayer and it can be labeled by DiI, the labeled groups of fluorescent liposomes are co-incubated with cells for different times, after analyzed by flow cytometry, the uptake of each group of preparations by cells can be determined. Transferrin is a ligand with the transferrin receptor on the cell surface, and the transferrin receptor on the surface of tumor cells is highly expressed. Therefore, modifying transferrin on the surface of the preparation can achieve a certain effect of targeting the tumor site, and transferrin can mediate the endocytic uptake of cells[18]. The results of cellular uptake experiments were shown in **Fig. 3A&3B**, after 2 h of co-incubation, the uptake rates of DiI, DiI@Lip and DiI@Tf-Lip were 17.4%, 28.7% and 36.5%, after 4 h of co-incubation, the uptake rates of DiI, DiI@Lip and DiI@Tf-Lip were 32.1%, 47.7% and 67.7%, after 8 h of co-incubation, the uptake rates of DiI, DiI@Lip and DiI@Tf-Lip were 44.6%, 72.8% and 85.1%. After 4 and 8 h of incubation, there was a significant difference in the uptake rate of DiI@Lip and DiI@Tf-Lip in MCF-7 cells because modifying Tf on the surface of liposomes could target TfR in MCF-7 cells, improving the efficiency of cell uptake.

Confocal laser scanning microscopy (CLSM) was used to evaluate the cellular uptake of GA@Tf-Lip by MCF-7 cells after co-incubation for 8 h. The results are shown in **Fig. 3C&3D** with red fluorescence originating from the DiI. Semi-quantitative analysis showed that the cellular fluorescence of DiI@Tf-Lip was significantly higher than that of DiI and DiI@Lip, which was consistent with the results of cell flow cytometry. These results proved that GA@Tf-Lip could significantly enhance the cellular uptake of GA by MCF-7 cells owing to the Tf modification.

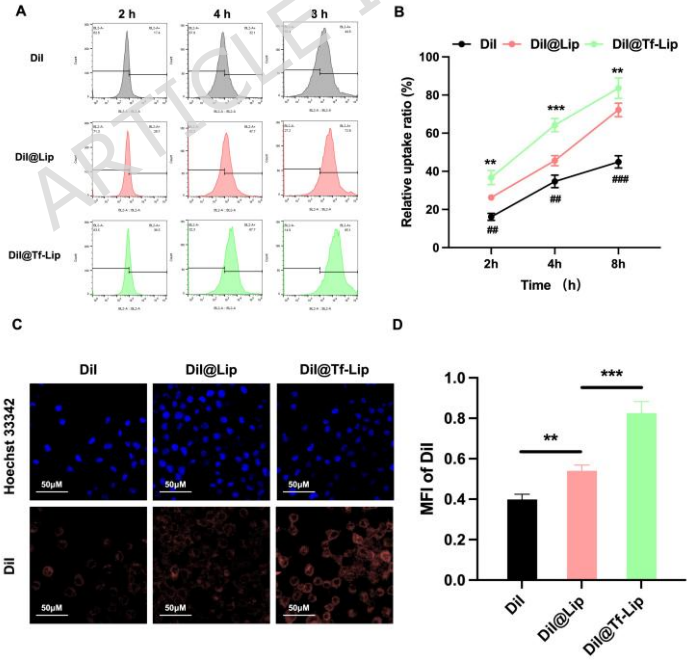

Fig. 3 Cellular uptake study of DiI@Tf-Lip by MCF-7 cells. (A) Cell flow cytometry results of cellular fluorescence in MCF-7 cells in different groups, (B) Cellular uptake rate of different preparations by MCF-7 cells (n = 3), (C) CLSM results of cellular uptake experiments (50 μm), (D) Semi-quantitative analysis of DiI (red) in CLSM pictures (n =3). (Significant difference: $^{*}P < 0.05$, $^{**}P < 0.01$, $^{***}P < 0.001$.)

3.4 Ability of GA@Tf-Lip to enhance ferroptosis in MCF-7 cells

3.4.1 Fe^{2+} content

Fe^{3+} can bind to Tf and enter the cell through TfR-mediated endocytosis, which is then reduced to Fe^{2+} and released into the cells[30]. Owing to the high reactivity of Fe^{2+}, a large number of hydroxyl radicals can be produced through the Fenton reaction to generate lipid ROS after reacting with unsaturated lipids on the cell membrane, thereby inducing cell ferroptosis. FerroOrange is a Fe^{2+}-specific fluorescent probe that can penetrate the cell membrane and bind to intracellular Fe^{2+} to produce orange fluorescence[31]. The results of intracellular Fe^{2+} content were shown in **Fig. 4A**, the intracellular Fe^{2+} content increased in each group. Compared with the Fe^{3+} and GA+Fe^{3+} groups, there was no significant difference in the Fe^{2+} content in the GA@Lip + Fe^{3+} group, whereas the Fe^{2+} content in the GA@Tf-Lip + Fe^{3+} group was significantly increased. The accumulation of Fe^{2+} in the GA@Tf-Lip + Fe^{3+} group was 1.3 times of the GA@Lip + Fe^{3+} group because the Tf-modified surface could target the TfRs of tumor cells and enhance cytosis by participating in the Tf cycle of cells, promoting the accumulation of intracellular Fe^{2+} to efficiently induce ferroptosis.

3.4.2 MDA analysis

MDA is the final product of lipid peroxidation in organisms and is an important indicator of the level of lipid peroxidation and oxidative stress. As a result, the higher the intracellular MDA content, the more susceptible a cell is to ferroptosis. The results of intracellular MDA content of **Fig. 4B**, the MDA content of the GA@Tf-Lip group, and the MDA content of the GA@Tf-Lip + Fe^{3+} group increased by approximately 2.1 times compared to that of the GA group, indicating that transferrin-modified liposomes significantly increased the accumulation of intracellular peroxide and promoted ferroptosis in tumor cells.

3.4.3 GSH analysis

GSH is an antioxidant present in cells that has many abilities, including clearing reactive oxygen species, preventing lipid peroxidation, metabolizing peroxides and heavy metals, and preventing cellular oxidative stress. The lower the level of GSH in the cell, the greater the sensitivity to ferroptosis. The results of intracellular GSH content were shown in **Fig. 4C**, compared to the Control group, the intracellular GSH content of MCF-7 was significantly reduced in each other groups, including 76.81 ± 5.94% in the GA group, 72.37 ± 4.48% in the GA@Lip group, 60.62 ± 4.58% in the GA@Tf-Lip group, and 47.20 ± 5.94% in the GA@Tf-Lip+Fe^{3+} group. The results showed that Tf-modified liposomes greatly increased the GSH depletion rate and promoted ferroptosis in tumor cells.

3.4.4 GPX4 analysis

GPX4 is highly expressed in tumor cells and can remove lipid peroxide in cells, which is an important indicator of ferroptosis. Cells with ferroptosis often inactivate GPX4. The GPX4 expression results were shown in **Fig. 4D** and the original blots/gels are presented in Supplementary **Fig. S1**. Compared with the Control group, the GPX4 protein level in the GA group decreased by 21.7%, The GPX4 expression in the GA@Lip group was 55.0% compared to the Control group. The GA@Tf-Lip group had the greatest effect on downregulating GPX4 protein, which was only 46.6% of the control group. There was also a significant difference between the GA@Lip and GA@Tf-Lip groups, which proved that the Tf-modified liposomes were more effective in inducing ferroptosis.

3.4.5 Cell mitochondrial membrane potential analysis

Mitochondria are important components of cellular energy and metabolism, and normal cells have a high mitochondrial membrane potential, maintaining a positive and negative physiological state[32]. When ferroptosis occurs in cells, the electron transport process of mitochondria is impaired, resulting in a decrease in the mitochondrial membrane potential and depolarization. JC-1 is a fluorescent probe that is widely used to detect mitochondrial membrane potential. When the mitochondrial membrane potential is high, JC-1 produces red fluorescence; when the mitochondrial membrane potential decreases, JC-1 produces green fluorescence. The mitochondrial membrane potential results are shown in **Fig. 4E**, which show to GA group, the green fluorescence of the GA@Tf-Lip + Fe^{3+} group was significantly enhanced. The ability of GA@Lip to induce a decrease in mitochondrial membrane potential was 1.4 times and the ability of GA@Tf-Lip to induce a decrease in mitochondrial membrane potential was 1.8 times free GA. In the iron-containing microenvironment, the ability of GA@Tf-Lip to induce mitochondrial membrane potential reduction was significantly enhanced which was 1.9 times of GA@Tf-Lip in the low-iron environment. These results suggest that GA@Tf-Lip can significantly reduce or even eliminate the mitochondrial membrane potential in the iron-containing tumor microenvironment and promote ferroptosis.

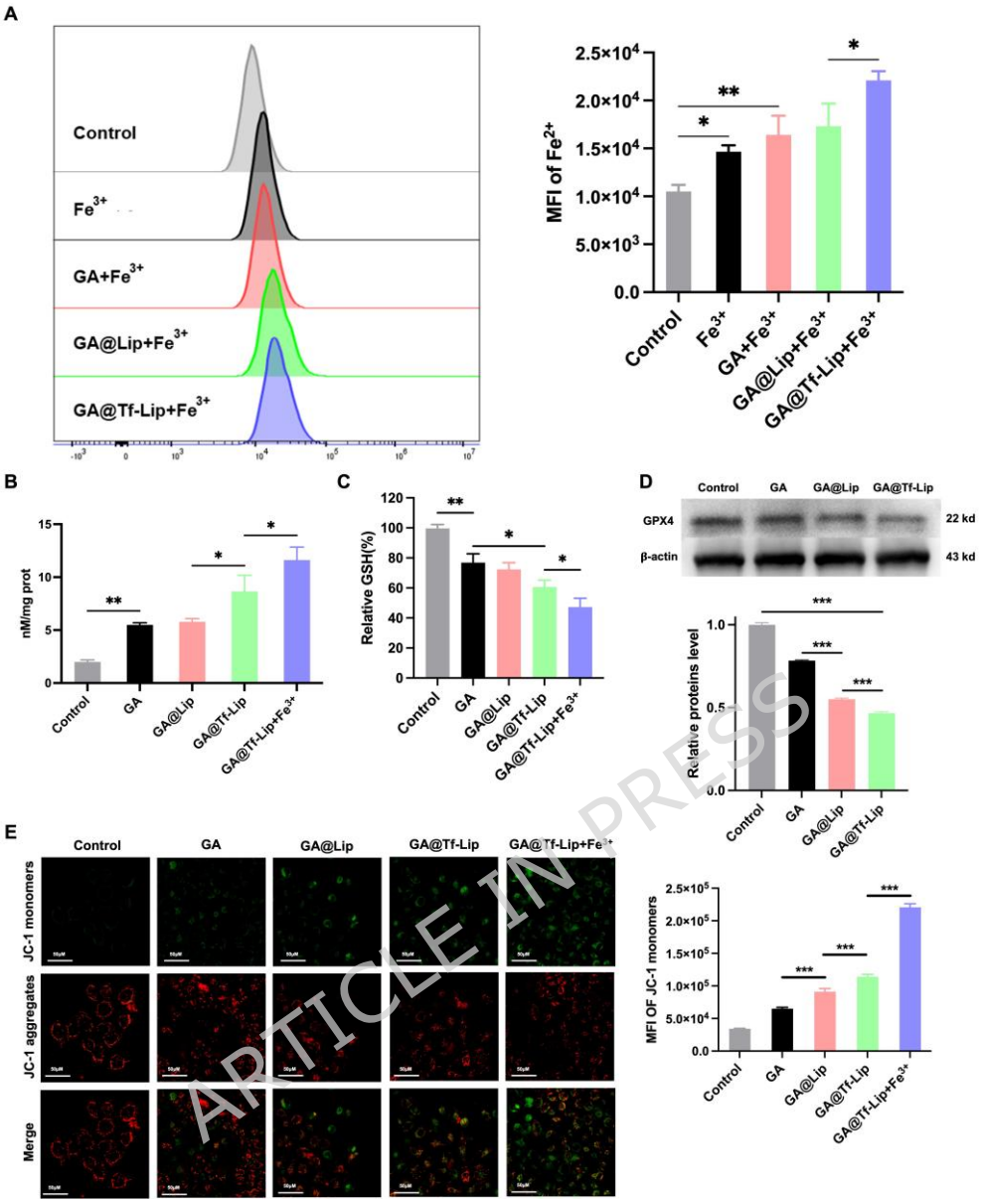

Fig. 4 The ability of GA@Tf-Lip to promote ferroptosis in MCF-7 cells. The influence of GA@Tf-Lip on the Fe^{2+} concentration (A), MDA (B), GSH (C), GPX4 (D) and mitochondrial membrane potential (E) in MCF-7 cells (n =3). (Significant difference: $^{*}P < 0.05$, $^{**}P < 0.005$, $^{***}P < 0.001$.)

3.5 *In vitro* safety evaluation

3.5.1 Hemolysis study

Prior to *in vivo* pharmacodynamic experiments, a safety investigation is required. GA and its preparations were tail vein injections to conduct a hemolysis study. The results of *in vitro* hemolysis study were shown in **Fig. S2**, the hemolysis rates of pure water, PBS, GA, GA@Lip and GA@Tf-Lip were 99.8 ± 0.1%, 1.7 ± 0.2%, 1.7 ± 0.1%, 1.7 ± 0.1% and 1.7 ± 0.2%, respectively. The hemolysis rate of intravenous drugs should be less than 5%, and the prepared preparations meet the requirements of intravenous injection and can be used for tail vein administration in animals.

3.5.2 Vascular irritation experiments

According to the H&E staining results of rabbits from different groups (**Fig. S3**), the vascular wall of rabbit ears from the saline group was intact, the tissues of all layers were normal with no swelling, necrosis, or shedding of rabbit ear vascular endothelial cells, and there was no thrombosis, congestion, edema, hemorrhage, or inflammatory cell infiltration. Tissue swelling, bleeding, and accumulation of inflammatory cells were observed in the GA group, indicating that GA caused vascular irritation. Compared with the GA group, there were no obvious lesions or inflammation in the GA@Lip and GA@Tf-Lip groups, indicating that the prepared GA@Lip and GA@Tf-Lip could decrease the vascular irritation of GA.

3.6 *In vivo* distribution investigation

The results of the distribution of different preparations *in vivo* are shown in **Fig. 5A&5B**, Fluorescence was rapidly distributed in mice within 1 h, with the highest level, and was mainly concentrated in the abdomen of mice. ICG was rapidly metabolized, the fluorescence intensity was reduced at 4 h, and there was no obvious fluorescence at 8 h. However, the fluorescence intensity of the ICG@Lip and ICG@Tf-Lip groups showed a slow downward trend between 1 and 6 h, indicating that the liposome could prolong the *in vivo* circulation time. ImageJ software was used to determine the mean fluorescence intensity (MFI) in tumors, and the results are shown in **Fig. 5C**. Semi-quantitative results showed that the fluorescence intensity of tumors in the ICG@Tf-Lip group was higher than that in the ICG@Lip group, indicating better tumor-targeting drug release ability. The fluorescence intensities of the tumors, liver, and kidney in the ICG group were the lowest, indicating that ICG was metabolized in large quantities after 24 h. Semi-quantitative analysis of liver fluorescence intensity was also conducted and the results are shown in **Fig. S4**. In Conclusion, the tumors and livers of the ICG@Lip and ICG@Tf-Lip groups still showed obvious fluorescence, and the fluorescence of the tumor site in the ICG@Tf-Lip group was stronger than that in the ICG@Lip group, whereas the fluorescence of the liver was weaker than that in the ICG@Lip group, indicating that transferrin modification enhanced the targeting of liposomes to the tumor site and reduced drug accumulation in the liver.

3.7 Evaluation of anti-tumor effects of GA@Tf-Lip *in vivo*

After administration of saline, DOX, GA, GA@Lip, and GA@Tf-Lip, the weight of the mice, tumor volume, and tumor weight were recorded, and the results are shown in **Fig. 5D-5G**. There are normal weight increases in all groups without significant fluctuations. Additionally, H&E staining results of main organs from different groups are shown in **Fig. S5**, which reveals no pathological damage such as lesions or necrosis, indicating that the *in vivo* safety of GA@Tf-Lip. There are various size of the tumor in diameter in each group, control group have the biggest size of 1.556 ± 0.241 cm in diameter, DOX group have a size of 1.025 ± 0.160 cm in diameter, GA group have a size of 1.398 ± 0.151 cm in diameter, GA@Lip group have a size of 1.092 ± 0.183 cm in diameter, while GA@Tf-Lip group have the smallest size of 0.720 ± 0.064 cm in diameter. After administration, the tumor volume in the Control group was the largest (1228.9 ± 103.3 mm^3), with a highest tumor weight (1.19 ± 0.10 g). The tumor volume in the DOX group was 240.5 ± 25.7 mm^3 and the tumor weight was 0.24 ± 0.03 g, indicating an efficient anti-tumor effect *in vivo*. The tumor volume of the GA group and the GA@Lip group were 606.6 ± 39.3 mm^3 and 411.1 ± 58.9 mm^3, the tumor weight was 0.62 ± 0.06 g and 0.43 ± 0.05 g, respectively. This demonstrated that GA@Lip had a stronger inhibitory effect on solid tumors than GA, which might be due to liposomes prolonging the circulation time of drugs in the body and improving their bioavailability. The tumor volume of the GA@Tf-Lip group was smallest (137.3 ±

13.1 mm^3) with a lightest tumor weight (0.13 ± 0.02 g), indicating that modifying Tf on the surface of liposomes might promote GA-induced ferroptosis by enhancing the tumor-targeting effect and enhancing ferroptosis in tumor cells.

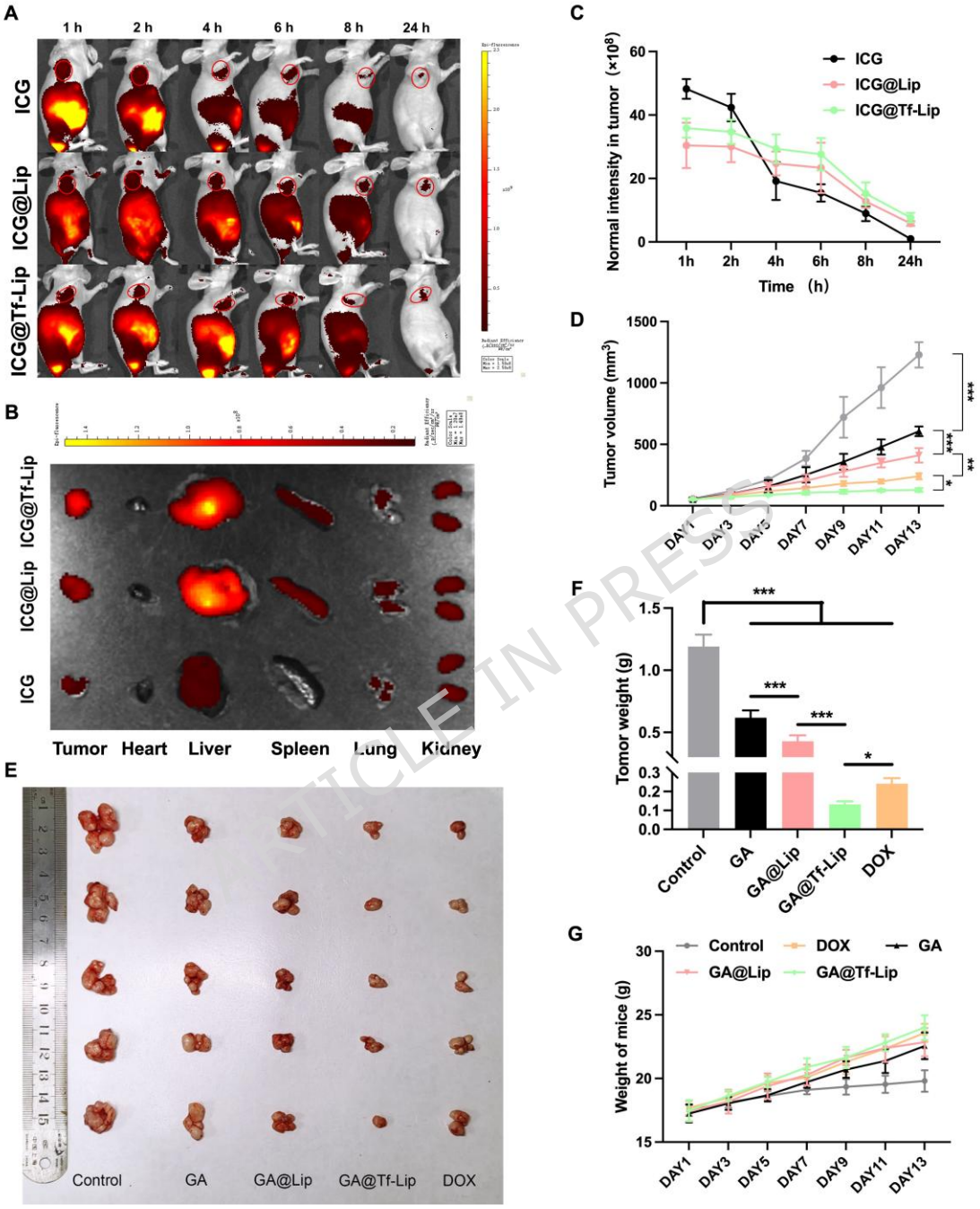

Fig. 5 *In vivo* evaluation of GA@Tf-Lip in tumor-bearing mice. (A) *In vivo* images of MCF-7 bearing mice following injection of different fluorescently labeled liposomes (n = 3). (B) *Ex vivo* images of the tumors and organs from MCF-7 bearing mice (n = 3). (C) The mean fluorescent intensity of ICG in the tumor *in vivo* (n = 3). (D) The volume of tumors (n = 8). (E) Pictures of tumors. (F) The weight of tumors (n = 8). (G) Body weight changes of the mice (n = 8). (Significant difference: $^{*}P < 0.05$, $^{**}P < 0.005$, $^{***}P < 0.001$.)

To investigate the ability of different preparations to induce ferroptosis in tumor cells *in vivo*, the tumors in each group were analyzed using frozen fluorescent sections, and the results are shown in **Fig. 6**. As shown in **Fig. 6A**, FerroOrange was used to stain Fe^{2+} (red fluorescence), DCFH-DA was related to ROS (red fluorescence), and Liperfluo represented the level of LPO (green fluorescence). According to the semi-quantitative results shown in **Fig. 6B-6D**, ferroptosis-related factors were all increased after administration. The Fe^{2+} concentration in the GA@Tf-Lip group was 3.14 times higher than that in the GA@Lip, 1.23 times higher than that in the DOX group. The level of ROS in the GA group was 3.8 times higher than that in the control group, indicating that GA increases the production and accumulation of ROS to promote ferroptosis. Compared to the GA group, the levels of ROS in the DOX, GA@Lip, and GA@Tf-Lip group were 2.8 times, 1.3 times and 3.2 times higher. The LPO level in the GA@Lip group was 1.9 times higher than that in the GA group, whereas the level of LPO in the GA@Tf-Lip group was 1.8 times higher than that in the GA@Lip group.

The results of Ki67 and GPX4 staining of the tumor tissues are shown in **Fig. 6E**. Ki67 was highly expressed in tissues with high cell proliferation activity, and GPX4 was a significant factor related to ferroptosis resistance, whereas the brown parts were Ki67 and GPX4 positive. According to the semi-quantitative results in **Fig. 6F&6G**, compared to the control group, the levels of GPX4 and Ki67 decreased significantly after administration. For Ki67, GA@Lip and GA@Tf-Lip significantly decreased Ki67 levels, and GA@Tf-Lip had the best effect. For GPX4, the relative protein levels in the GA, GA@Lip, GA@Tf-Lip, and DOX group were 74.53%, 34.04%, 20.11% and 80.84%, which represents that GA can decrease the expression of GPX4 to induce ferroptosis in tumors *in vivo*, and the Tf modification significantly enhanced this therapeutic effect owing to the ability of the better tumor targeting ability.

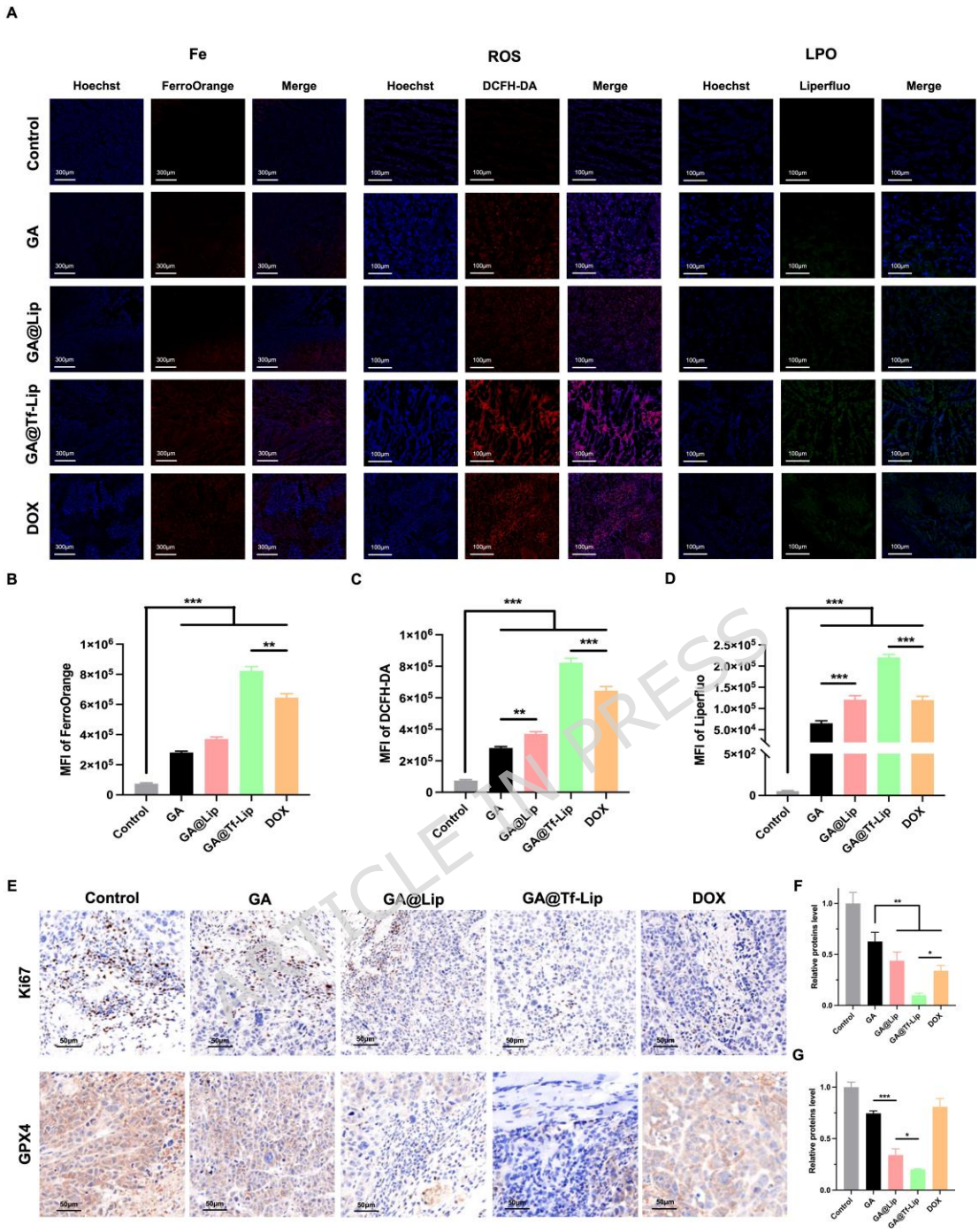

Fig. 6 The ability of GA@Tf-Lip to induce ferroptosis in tumors *in vivo*. (A) Immunofluorescent sections of tumor issues by FerroOrange, DCFH-DA and Liperfluo staining. (B) Semi-quantitative results of Fe^{2+} concentration (C), the levels of ROS (D), and LPO (E) Immunofluorescent sections of tumor isjsues by Ki67 and GPX4 staining. (F) Semi-quantitative results of the levels of Ki67 (F) and GPX4 (G). (Significant difference: $^{*}P < 0.05$, $^{**}P < 0.005$, $^{***}P < 0.001$.)

In conclusion, the prepared GA@Tf-Lip had a greater ability to induce ferroptosis in tumor tissues *in vivo* than DOX, GA, and GA@Lip. It can significantly increase ferroptosis-inducing factors, including Fe^{2+} uptake, ROS production, and LPO accumulation, and decrease the levels of GPX4 and Ki67, which are related to ferroptosis resistance and tumor growth.

Several limitations of this study should be acknowledged. First, although Tf modification enhances tumor targeting, TfR is also expressed in some normal tissues and cells, which may lead to potential off-target risks. Second, the potential immunogenicity of Tf-modified liposomes remains to be evaluated, as repeated administration may elicit anti-Tf antibody responses, potentially limiting clinical translation. Third, comprehensive *in vivo* toxicity evaluations, including long-term safety and pharmacokinetic profiles, are necessary before further development. Future studies should address these issues through immunogenicity assays, repeated-dose toxicity studies, and the exploration of alternative targeting ligands with lower immunogenic potential.

4 Conclusion

In summary, we developed GA-loaded Tf-modified pH-responsive liposomes (GA@Tf-Lip) for BC treatment. pH-sensitive DOPE was used to construct liposomes to disintegrate GA@Tf-Lip at acidic tumor sites. Specifically, Tf-modification enhanced the tumor-targeting ability of GA@Tf-Lip and promoted Fe^{2+} accumulation in tumor cells. GA@Tf-Lip also effectively induced ferroptosis in tumor cells, which solved the limitations of GA in cancer treatment, such as poor water solubility and vascular irritation. Overall, the developed GA@Tf-Lip is an ideal therapeutic nanomedicine and provides a new approach for the treatment of BC and the clinical application of GA.

Data Availability Statement

The data supporting the findings of this study are available from the corresponding author upon reasonable request.

Ethics Approval and Informed Consent

All animal experimental protocols were approved by the Institutional Animal Care and Use Committee of Shanghai University of Traditional Chinese Medicine (PZSHUTCM2309080007, PZSHUTCM2309110010). All experiments were performed in accordance with the Guidelines for the Care and Use of Laboratory Animals of Shanghai University of Traditional Chinese Medicine. At the end of the experiments, the mice were euthanized by intraperitoneal injection of excessive 1.25% tribromoethanol (20 μL/g), the rabbits were euthanized via intraperitoneal injection injection of excessive soidum pentobarbital (100 mg/kg). Authors confirmed that all animal experiments were performed in accordance with ARRIVE guidelines.

Acknowledgments

Funding

This work was financially supported by Programs of the National Natural Science Foundation of China (grant number 82274066); National Key Research and Development Program of China (grant 2022YFC3501705); Shanghai Leading Talent (grant number 2019100); Program of Shanghai Academic/Technology Research Leader (grant 22XD1423000); “Shuguang Program” supported by Shanghai Education Development Foundation and Shanghai Municipal Education Commission (grant

number 20SG43); Project from Shanghai Committee of Science and Technology (grant number 22S21901200 and 21010504200); Youth Talent Program from the Shanghai Municipal Health Commission (Grant 2022YQ030); Natural Science Foundation of Shanghai (grant number 21ZR1460800 and 22ZR1459000).

CRediT authorship contribution statement

Wenqing Rong: Writing - original draft, Writing – review and editing, Formal Analysis, Data Curation, Investigation. **Minquan Zhang**: Writing - original draft, Writing – review and editing, Formal Analysis, Data Curation, Investigation. **Siqi Yang**: Writing - original draft, Writing-review and editing, Formal Analysis, Data Curation, Investigation. **Kaiwen Wang**: Writing – review and editing, Conceptualization, Investigation, Formal analysis. **Xiaoping Yang**: Writing – review and editing, Investigation, Formal analysis. **Guolei Zhang**: Writing – review and editing, Visualization, Investigation. **Zhe Li**: Writing – review and editing, Conceptualization, Methodology, Visualization. **Yue Ding**: Writing – review and editing, Resources, Funding acquisition, Methodology. **Tong Zhang**: Writing – review and editing, Project administration, Supervision, Resources, Methodology, Funding acquisition, Conceptualization. **Yun Gai**: Writing – review and editing, Project administration, Supervision, Resources, Methodology, Funding acquisition, Conceptualization. **Jinshuai Lan**: Writing – review and editing, Supervision, Funding acquisition, Resources, Project administration, Methodology, Conceptualization

Declaration of competing interest

The authors declare that they have no known competing financial interests or personal relationships that could have appeared to influence the work reported in this paper.

References

1. Feng, Y. *et al.* Breast cancer development and progression: Risk factors, cancer stem cells, signaling pathways, genomics, and molecular pathogenesis. *GENES Dis.* **5**, 77–106 (2018).

2. Liao, L. Inequality in breast cancer: Global statistics from 2022 to 2050. *BREAST* **79**, 103851 (2025).

3. Arnold, M. *et al.* Current and future burden of breast cancer: Global statistics for 2020 and 2040. *BREAST* **66**, 15–23 (2022).

4. Zhai, J., Wu, Y., Ma, F., Kaklamani, V. & Xu, B. Advances in medical treatment of breast cancer in 2022. *Cancer Innov.* **2**, 1–17 (2023).

5. Ge, A. *et al.* Broadening horizons: the multifaceted role of ferroptosis in breast cancer. *Front. Immunol.* **15**, 1455741 (2024).

6. Zhang, M. Q. *et al.* Ferroptosis meets biomimetic nano-systems: A novel strategy for targeted cancer therapy. *Cell Biomater.* **1**, 100023 (2025).

7. Zheng, J. *et al.* Sorafenib fails to trigger ferroptosis across a wide range of cancer cell lines. *CELL DEATH Dis.* **12**, 698 (2021).

8. Pan, X. *et al.* Erastin decreases radioresistance of NSCLC cells partially by inducing GPX4-mediated ferroptosis. *Oncol. Lett.* **17**, 3001–3008 (2019).

9. Sui, X. *et al.* RSL3 Drives Ferroptosis Through GPX4 Inactivation and ROS Production in Colorectal Cancer. *Front. Pharmacol.* **9**, 1371 (2018).

10. Liang, X. *et al.* Metal-organic framework-based photodynamic combined immunotherapy against the distant development of triple-negative breast cancer. *Biomater. Res.* **27**, 120 (2023).

11. Rashidzadeh, H. *et al.* Preparation of alginate coated Pt nanoparticle for radiosensitization of breast cancer tumor. *Int. J. Biol. Macromol.* **233**, 123273 (2023).

12. Xia, C. *et al.* Sponge-like nano-system suppresses tumor recurrence and metastasis by restraining myeloid-derived suppressor cells-mediated immunosuppression and formation of pre-metastatic niche. *ACTA Biomater.* **158**, 708–724 (2023).

13. Zhang, Y. *et al.* Versatile metal-phenolic network nanoparticles for multitargeted combination therapy and magnetic resonance tracing in glioblastoma. *BIOMATERIALS* **278**, 121163 (2021).

14. Zhang, Y. *et al.* Glioblastoma Therapy Using Codelivery of Cisplatin and Glutathione Peroxidase Targeting siRNA from Iron Oxide Nanoparticles. *ACS Appl. Mater. INTERFACES* **12**, 43408–43421 (2020).

15. Chen, H. & Wen, J. Iron oxide nanoparticles loaded with paclitaxel inhibits glioblastoma by enhancing autophagy-dependent ferroptosis pathway. *Eur. J. Pharmacol.* **921**, 174860 (2022).

16. Hatami, E., Jaggi, M., Chauhan, S. C. & Yallapu, M. M. Gambogic acid: A shining natural compound to nanomedicine for cancer therapeutics. *Biochim. Biophys. ACTA-Rev. CANCER* **1874**, 188381 (2020).

17. Jing, Y. *et al.* Development of a manganese complex hyaluronic acid hydrogel encapsulating stimuli-responsive Gambogic acid nanoparticles for targeted Intratumoral delivery. *Int. J. Biol. Macromol.* **270**, 132348 (2024).

18. Miller, L. D. *et al.* An Iron Regulatory Gene Signature Predicts Outcome in Breast Cancer. *CANCER Res.* **71**, 6728–6737 (2011).

19. de Oliveira, M. C. *et al.* pH-sensitive liposomes as a carrier for oligonucleotides: a physico-chemical study of the interaction between DOPE and a 15-mer oligonucleotide in excess water. *Biophys. Chem.* **87**, 127–137 (2000).

20. Lan, J. *et al.* Shuttle-like Fe(III)-gambogic acid nanoassemblies: disrupting intracellular redox balance and enhancing tumor penetration to amplify ferroptosis therapy of large tumors. *Adv. Compos. HYBRID Mater.* **8**, 338 (2025).

21. Ma, Z. *et al.* Enhanced Anticancer Efficacy of Dual Drug-Loaded Self-Assembled Nanostructured Lipid Carriers Mediated by pH-Responsive Folic Acid and Human-Derived Cell Penetrating Peptide dNP2. *PHARMACEUTICS* **13**, 600 (2021).

22. Lan, J. *et al.* Unlocking the anticancer activity of gambogic acid: a shift towards ferroptosis via a GSH/Trx dual antioxidant system. *FREE Radic. Biol. Med.* **218**, 26–40 (2024).

23. Alic, L., Binder, C. J. & Papac-Milicevic, N. The OSE complotype and its clinical potential. *Front. Immunol.* **13**, 1010893 (2022).

24. Yang, W. S. *et al.* Regulation of Ferroptotic Cancer Cell Death by GPX4. *CELL* **156**, 317–331 (2014).

25. Chen, Y., Zhang, P., Chen, W. & Chen, G. Ferroptosis mediated DSS-induced ulcerative colitis associated with Nrf2/HO-1 signaling pathway. *Immunol. Lett.* **225**, 9–15 (2020).

26. Chen, L., Hambright, W. S., Na, R. & Ran, Q. Ablation of the Ferroptosis Inhibitor Glutathione Peroxidase 4 in Neurons Results in Rapid Motor Neuron Degeneration and Paralysis. *J. Biol. Chem.* **290**, 28097–28106 (2015).

27. Nijhawan, H. P., Shyamsundar, P., Prabhakar, B. & Yadav, K. S. PEGylated pH-Responsive Liposomes for Enhancing the Intracellular Uptake and Cytotoxicity of Paclitaxel in MCF-7 Breast Cancer Cells. *AAPS PHARMSCITECH* **25**, 216 (2024).

28. Uggeri, J. *et al.* Calcein-AM is a detector of intracellular oxidative activity. *Histochem. CELL Biol.* **122**, 499–505 (2004).

29. Krapoth, T. C. *et al.* Wanted: Dead or Alive Cells with Propidium Iodide Staining in Liver Tissue. *Int. J. Mol. Sci.* **25**, 13521 (2024).

30. Guan, Z. *et al.* Self-enhanced targeted nanomedicines based on iron starvation acclimation for tumor-specific therapy. *Chem. Eng. J.* **495**, 153371 (2024).

31. Grubwieser, P. *et al.* Quantification of Macrophage Cellular Ferrous Iron (Fe2+) Content Using a Highly Specific Fluorescent Probe in a Plate Reader. *Bio-Protoc.* **14**, e4929 (2024).

32. Pedrera, L. *et al.* Ferroptosis triggers mitochondrial fragmentation via Drp1 activation. *CELL DEATH Dis.* **16**, 40 (2025).